ANNUAL REVIEWS

Annual Review of Analytical Chemistry

Flow Cytometric Analysis of Nanoscale Biological Particles and Organelles

Hong Lian,* Shengbin He,* Chaoxiang Chen, and Xiaomei Yan

MOE Key Laboratory of Spectrochemical Analysis and Instrumentation; Key Laboratory for Chemical Biology of Fujian Province; Collaborative Innovation Center of Chemistry for Energy Material; and Department of Chemical Biology, College of Chemistry and Engineering, Xiamen University, Xiamen, Fujian 361005, China; email: xmyan@xmu.edu.cn

Annu. Rev. Anal. Chem. 2019. 12:389–409

First published as a Review in Advance on April 12, 2019

The *Annual Review of Analytical Chemistry* is online at anchem.annualreviews.org

https://doi.org/10.1146/annurev-anchem-061318-115042

*These authors contributed equally to this article.

Keywords

single-particle analysis, flow cytometry, bacteria, mitochondria, viruses, extracellular vesicles

Abstract

Analysis of nanoscale biological particles and organelles (BPOs) at the single-particle level is fundamental to the in-depth study of biosciences. Flow cytometry is a versatile technique that has been well-established for the analysis of eukaryotic cells, yet conventional flow cytometry can hardly meet the sensitivity requirement for nanoscale BPOs. Recent advances in high-sensitivity flow cytometry have made it possible to conduct precise, sensitive, and specific analyses of nanoscale BPOs, with exceptional benefits for bacteria, mitochondria, viruses, and extracellular vesicles (EVs). In this article, we discuss the significance, challenges, and efforts toward sensitivity enhancement, followed by the introduction of flow cytometric analysis of nanoscale BPOs. With the development of the nano-flow cytometer that can detect single viruses and EVs as small as 27 nm and 40 nm, respectively, more exciting applications in nanoscale BPO analysis can be envisioned.

1. INTRODUCTION

Analysis of biological particles and organelles (BPOs) at the single-particle level provides unprecedented new insights into biological, biomedical, and environmental sciences, as variability or heterogeneity is an intrinsic property of BPOs that is implicated in cellular evolution, environmental adaptation, and ecological equilibrium (1–5). Because most BPOs, such as bacteria, viruses, subcellular organelles, and extracellular vesicles (EVs), are individually nanoscale in size (with at least one dimension smaller than 1,000 nm), they are usually analyzed on a bulk basis with heterogeneity masked by ensemble-averaged measurements. Therefore, single-particle techniques with high sensitivity, high throughput, and multiparameter capability are urgently needed to reveal the heterogeneity of nanoscale BPOs and to decipher the correlations among different attributes. Compared with numerous technologies for single BPO analysis, such as electron microscopy (6), fluorescence microscopy (7), atomic force microscopy (8), and surface plasmon resonance microscopy (9), flow cytometry can easily fulfill all the aforementioned requirements and exhibits advantages regarding statistical robustness and convenience of use.

However, conventional flow cytometers designed for the analysis of eukaryotic cells can hardly provide enough sensitivity for the analysis of nanoscale BPOs. Nevertheless, great efforts have been made to increase the performance of flow cytometers. There have been many instrumental advances along the way, ultimately leading to the flow cytometric detection of single viruses and EVs down to 27 nm and 40 nm, respectively (10, 11). This article reviews recent advances of flow cytometry in the analysis of single nanoscale BPOs with specific focus on the measurements of bacteria, mitochondria, viruses, and EVs. We highlight and illustrate the instrumental advantages of several dedicated (or new generation) flow cytometers with improved sensitivity and resolution over conventional flow cytometers. In particular, using our laboratory-built nanoflow cytometer (nFCM) as a representative model (12–14), we elucidate the principles to achieve ultrasensitive detection of single nanoscale BPOs. Other flow cytometry variants such as mass cytometry (15, 16), imaging flow cytometry (17, 18), and microfluidic flow cytometry (19) are beyond the scope of this review, although they are undoubtedly important components of advanced flow cytometry.

2. THE SIGNIFICANCE OF INSTRUMENT SENSITIVITY

A flow cytometer works by guiding particles to flow into a hydrodynamically focused fluid stream, which runs with a sheath fluid surrounding the core sample stream (20–23). Particles confined in the core stream are subjected to one-by-one illumination by the laser beam to scatter light and emit fluorescence. Light scattered at relatively small angles, or forward-scattered (FSC) light, is collected almost parallel to the laser beam, while large-angle scattered light, or side-scattered (SSC) light and fluorescence, are collected in the direction perpendicular to the laser beam by separate detectors. If necessary, fluorescence-activated cell sorting may be used to obtain subpopulations of interest for further research. However, all cases require the signal of a particle to be discerned from the background, which is quite challenging when using conventional flow cytometers for nanoscale BPO analysis.

As light can be scattered by any particles with a refractive index different from the surrounding medium, light scattering is an essential parameter of flow cytometry not only in measuring the size and internal structure of biological particles but also in assessing the labeling ratios of subpopulations upon specific fluorescent staining. For conventional flow cytometers, the light-scattering detection limit is typically approximately 200–500 nm for polystyrene beads with refractive index of 1.59 (24, 25). As the refractive index of biological particles is much smaller, i.e., approximately 1.38–1.45 for bacteria (26), 1.40 for EVs (27), and 1.45–1.46 for viruses (10), the light-scattering

detection limit of BPOs is much larger. For example, according to Mie calculations, a polystyrene microsphere of 0.4 μm in diameter produced the same forward scatter intensity as a 1-μm lipid or cellular microparticle (28). Using a laboratory-built nFCM equipped with photomultiplier tubes (PMTs), we observed that the median SSC intensities of *Escherichia coli* (~1 μm) (29) and *Staphylococcus aureus* (~0.85 μm) (30) overlap mostly between those of 200-nm to 500-nm polystyrene beads (**Figure 1**). Not surprisingly, biological particles close to 1 μm could be partially beyond the scope of conventional flow cytometers by light-scattering detection, let alone the viruses (17–350 nm, with most close to or smaller than 100 nm) (24, 31). EVs (30 nm–1,000 nm, with most smaller than 150 nm) (11, 32) would utterly fall out of the detection range. Specifically, when the spherical particle is much smaller than the incident light wavelength, Rayleigh scattering theory applies, and the scattering intensity scales off with a sixth-power dependence of particle size as described below (33):

$$\sigma_{\text{scatt}} = \frac{2\pi^5 d^6 n_{\text{med}}^4}{3\lambda^4}\left|\frac{m^2-1}{m^2+2}\right|^2,$$

where σ_{scatt} is the scattering cross section, d is the particle diameter, λ is the wavelength of the incident light, n_{med} is the refractive index of the medium surrounding the particle, and m is the ratio of the refractive indices of the particle ($n_{\text{particle}} = n_{\text{rel}} + in_{\text{im}}$) and the medium ($n_{\text{med}}$). Based on the calculated σ_{scatt}, detecting single BPOs smaller than 100 nm is extremely challenging because pushing the detection limit from 200 nm down to 100 nm, 40 nm, and 25 nm corresponds to an approximately 64-, 15,625-, and 262,144-fold increase of the signal-to-noise (S/N) ratio, respectively (**Figure 2*a***).

To facilitate identification of single BPOs by flow cytometry, fluorescent staining of specific biochemical constituents is usually implemented to resolve BPOs from the background and distinguish them from other particulate matter. However, on one hand, conventional flow cytometers can hardly detect the fluorescence signal less bright than several hundred fluorescent molecules. On the other hand, for instance, an EV measuring 100 nm in diameter may bear 10,000 times fewer surface molecules and 1,000,000 times fewer cellular contents ready for staining, compared with a 10-μm-sized cell from which it originates, assuming that both the EV and parental cell share similar densities of these biochemical constituents. In this case, the fluorescent signals from nanoscale BPOs will be orders of magnitude dimmer and overstep the lowest fluorescence detection limits of conventional flow cytometers (34).

3. SENSITIVITY ENHANCEMENT THROUGH BETTER INSTRUMENTATION: FROM OLDER TO MODERN COMMERCIAL MODELS

Since its conception and birth in the 1960s, flow cytometry has experienced significant growth, and the milestones leading to modern flow cytometry have been reviewed (23, 35, 36). Here, we pay our respects to the pioneering work that constructed highly sensitive flow cytometers engaged in nanoscale BPO analysis. In 1979, using a custom-built device, the Shapiro group (37) was able to distinguish bacteriophage T2 (~100 nm) from a reovirus top component by light scattering, while the reovirus top component was just discernible from background noise. Their instrument featured a slow flow design, an observation volume (defined as the overlap of the laser spot and sample stream from which light emission can be collected and focused onto the detector) on the order of 100 fL, and a laser illumination power of 100 mW. By creating a laminar flow on a microscope cover slip by means of a jet water onto the glass at low angle, Steen & Lindmo (38)

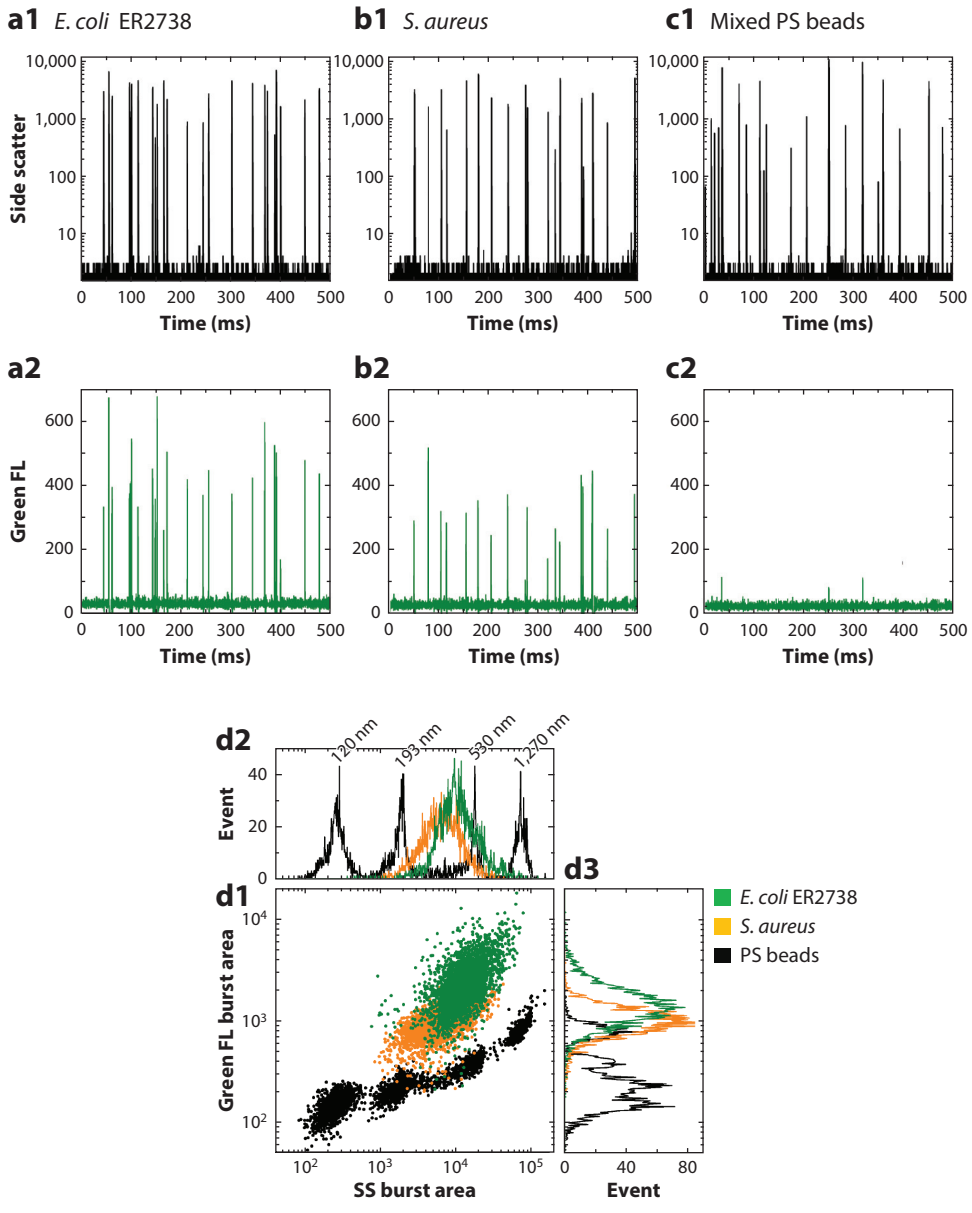

Figure 1

Light scatter and autofluorescence comparison between polystyrene (PS) beads and bacteria. (*a1*, *b1*, *c1*) Side scatter (SS) burst traces of *Escherichia coli* ER2738, *Staphylococcus aureus*, and mixed PS beads of different sizes. (*a2*, *b2*, *c2*) Green fluorescence (FL) burst traces for the above three samples. (*d*) Bivariate dot plots of the SS versus the FL burst area for the three samples.

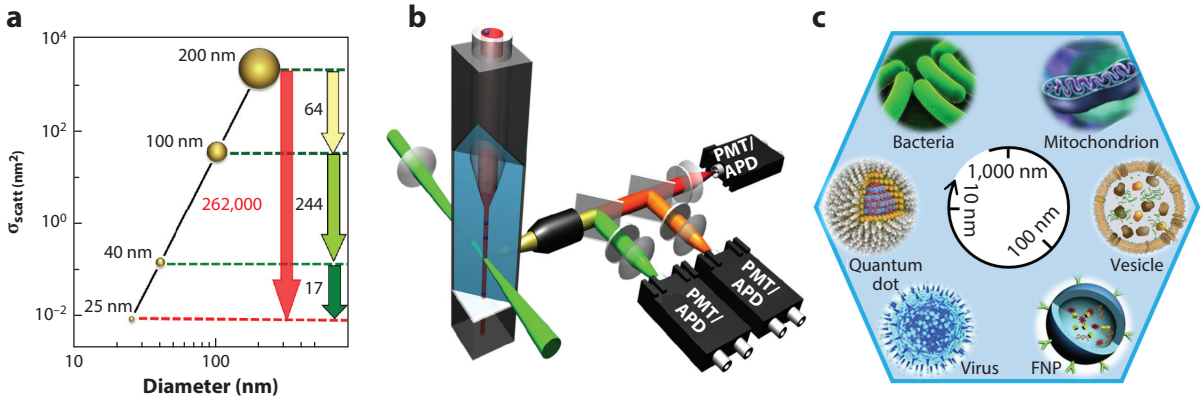

Figure 2

The laboratory-built nano-flow cytometer (nFCM) and its applications. (*a*) Relationship between the scattering cross section σ_{scatt} and particle diameter for silica nanoparticles at an excitation wavelength of 532 nm. (*b*) Schematic diagram of the laboratory-built apparatus. (*c*) Illustration of the nanoparticles that can be analyzed; nanoparticles not drawn to scale. Abbreviations: APD, avalanche photodiode; FNP, functional nanoparticle; PMT, photomultiplier tube. Figure adapted with permission from Reference 11. Copyright 2018, American Chemical Society.

developed a new flow configuration that can be implemented on a standard fluorescence microscope. A dark-field illumination configuration was then incorporated, smartly addressing the conflicts between the wide illumination field of the arc lamp and the arrangement of scattering detectors at various angles without sacrificing detection sensitivity. Such design permitted light-scattering measurement at a small angle (outward from approximately 2°) and a large angle (outward from approximately 18°) separately, both of which have a detection limit of approximately 200-nm polystyrene beads (39, 40). Later, on a modified laser-based flow cytometer, Steen (24) achieved the discrimination of 74-nm polystyrene beads and viruses with sizes of approximately 100 nm by collecting scattered light over an angle of 16°–70°. Besides the increased light collection efficiency, the fluidics system was also modified to enable recirculation of the sheath water through a series of high-grade filters (including 0.1-μm filters) to remove debris.

According to light-scattering theory, particles larger than the wavelength of incident light predominantly scatter light in a forward direction. However, as the particle size becomes smaller, the light-scattering angle becomes wider, and a greater fraction of light is scattered in a perpendicular direction, which is the case for nanoscale BPOs smaller than the illumination wavelength (25, 33, 41). Hence, to improve the light-scattering sensitivity for BPOs, a detector with a large collection angle or even SSC is preferred (42). Recently, some commercial efforts have been made to extend the application of flow cytometers in small-particle detection through a series of strategies, including large angle detectors, high-power lasers, high performance PMTs, and ultraviolet excitation. For example, a custom modified BD influx (equipped with a 200-mW 488-nm laser and PMTs) can clearly distinguish between 100-nm and 200-nm polystyrene beads by light-scattering measurement with a reduced wide-angle FSC light (15°–25°). The reduced wide-angle FSC light aims to raise the minimal detection angle from the original 2° to 15°, so that stray light from the angle smaller than 15° can be blocked to elevate the S/N ratio (43–45). The BC Gallios offers a new W2 option that minimizes the optical noise by differentially amplifying the light collected between 8° and 19° (46, 47). A demonstration of its performance was the complete FSC resolution between the 100-nm and 300-nm Megamix polystyrene beads (46). The BC MoFlo Astrios EQ can easily resolve 100-nm fluorescent polystyrene beads by both light-scattering and fluorescence

measurements (48). In particular, the Apogee series A30/40/50-Micro with a scatter sensitivity of a 100-nm polystyrene bead is designed for microbiological analysis while being suitable for other nanoparticles. These instruments were evolved from the Stene/Bio-Rad Bryte design (36) and provide at most three nonfixed light-scattering angle ranges that can be optimized for better resolution of small and dim particles (49). The advantages of the A30/40/50-Micro for measuring small BPOs has been demonstrated (28, 50, 51). All of these commercial efforts have contributed to the increasing prevalence of flow cytometry in nanoscale BPO analysis.

4. SINGLE-MOLECULE FLUORESCENCE DETECTION IN A SHEATHED FLOW PROMOTES THE DEVELOPMENT OF ULTRASENSITIVE FLOW CYTOMETRY

A group at Los Alamos National Laboratory has been well known not only for its great contribution to the birth and advancement of conventional flow cytometry (21, 22, 52–54) but also for its endeavors in single-molecule fluorescence detection (SMFD) in a sheathed flow (55–57). These researchers began the pursuit to detect single-fluorophore molecules in flow with Dovichi et al.'s work in 1983 (58) and progressed until they detected them in 1990 (59). A continuous wave laser can fulfill the detection of a large protein molecule, B-phycoerythrin (PE), at the single-molecule level (60); however, for detecting a single chromophore dye (rhodamine-6G, approximately 30 times less fluorescent than PE), pulsed excitation and time-gated detection need to be implemented to reject the scattered light from solvent in the probe volume (59). The main strategies of SMFD in a sheathed flow include reducing the probe volume to subpicoliter level for background reduction, extending transit time of each particle passing through the focused laser beam to milliseconds for increased photon generation, employing a high numerical-aperture optical system to improve light collection efficiency, and using photon burst detection with a single-photon-counting avalanche photodiode (APD). Most notably, employing a sheathed flow system to confine the sample stream and isolate it far from the wall of the flow channel is indispensable to probe volume reduction and to efficiently block the scattered light from cuvette windows (61).

Adopting strategies for SMFD in a sheathed flow, our laboratory has spent the last decade working on both the light-scattering and fluorescence analysis of single BPOs much smaller than 100 nm. Using PMTs and a single-photon-counting APD as the detector for side scattering and fluorescence detection, respectively, we reported a clear differentiation of 100-nm polystyrene beads from background via light-scattering detection and single-molecule fluorescence detection of PE molecules (S/N of 17) in 2009 with a probe volume of 0.8 pL (12). Although the S/N ratio for the detection of 100-nm polystyrene beads was improved to 104 by reducing the probe volume to 0.15 pL (62), orders of magnitude sensitivity enhancement is still required to detect single BPOs as small as a few tens of nanometers in diameter. To enable the application of APD for SSC detection that had been impeded by the easy saturation of background scattering, we used an infinity-corrected microscope objective and a focusing lens to restrict the field of view of the APD detector solely to the sample stream for very good background rejection. In combination with a further reduction of probe volume to ~10 fL along with a relatively high laser excitation energy density ($\sim 5.0 \times 10^5$ W/cm^2) to generate more scattered photons, we achieved light-scattering detection of individual silica and gold nanoparticles as small as 24 nm (S/N of 7) and 7 nm (S/N of 5) in diameter, respectively (14). This is the first report of direct light-scattering detection below the level of single fluorescence molecules, as the light-producing power of a 25-nm diameter silica nanoparticle is even weaker than that of a typical chromophore such as fluorescein isothiocyanate. The nFCM extends the applicability and versatility of flow cytometry from the micron and submicron size range of particles down to the particles much smaller than 100 nm, and the

sizing resolution is comparable to that of transmission electron microscopy (TEM) (14). More applications in the analysis of BPOs and synthetic nanoparticles can be envisioned (**Figure 2*b,c***).

5. FLOW CYTOMETRIC ANALYSIS OF SINGLE BACTERIA

The motivation for analyzing bacteria at the single-cell level lies in the large heterogeneity in molecular content and phenotypic characteristics of complex or clonal cell populations. Such heterogeneity plays important roles in the development of drug resistance, ecological environment balance, and gastrointestinal health and disease (63–67). By offering high-throughput, quantitative, and multiparameter analysis at the single-cell level, flow cytometry has been extensively applied in microbiological research, including characterization of bacterial physiological responses to antimicrobial treatments (68, 69), detection of pathogenic bacteria in food, water, and clinical samples (70–72), and study of environmental microbiology (73, 74). For example, flow cytometry has been used to evaluate bacterial membrane permeability, membrane potential, esterase activity, glucose uptake, and respiratory activity upon antimicrobial treatments (75–78). By using recombinant fluorescent proteins as in vivo markers, one can trace the bacterial horizontal gene transfer and even analyze protein–protein interaction in a bacterial adenylate cyclase two-hybrid system (79–81). Nevertheless, great challenges remain for conventional flow cytometry to analyze small sizes of bacteria or biochemical constituents of low abundance. For example, many bacteria in aquatic ecosystems exhibit a much smaller size and lower content of specific macromolecules than laboratory cultures (82, 83). **Figure 3** shows the flow cytometric analysis of bacteria upon nucleic acid staining by an Apogee-A40. Fluorescence correlation spectroscopy (FCS) measurement indicates that most of the natural microbial flora in carrot samples were smaller than the spiked *E. coli* cells. Meanwhile, the green fluorescence intensity (an indicative of nucleic acid content) for intact cells of natural microbial flora was also weaker than that of the spiked *E. coli* (84).

Since the first report of the nFCM developed in our laboratory in 2009 (12), bacterial analysis has become one of our focuses. Employing PicoGreen nucleic acid stain to distinguish bacterial cells from other impurity particles, we can rapidly quantify total bacterial concentration in drinking water and tea beverages with great accuracy (85). Using the combination of SYTO 9 (cell membrane permeable) and propidium iodide (which penetrates only bacteria with compromised membranes) nucleic acid dyes, rapid and accurate detection of lactic acid bacteria and their viability in probiotic products was achieved (86). Combining immunofluorescent labeling with nucleic acid staining, absolute and simultaneous quantification of specific pathogenic strain and total bacterial cells was demonstrated using a mixture of *E. coli* O157:H7 and *E. coli* DH5α (87).

The superior sensitivity of the nFCM also offers a great opportunity to characterize numerous biochemical properties of single bacteria that can hardly be analyzed using conventional flow cytometry. For example, we detected the very weak autofluorescence of single bacterial cells in the green region of the spectrum and quantified its brightness by calibrating against a series nanospheres with known FITC equivalents. It was found that the autofluorescence of a single bacterium can vary from an average of 80 FITC equivalents for *S. aureus* to 1,400 FITC equivalents for *Bacillus subtilis*, and there exists a relatively large cell-to-cell variation with a coefficient of variation ranging from 75% to 39% (88). Because β-galactosidase is a widely used cellular reporter for gene expression, we developed an ultrasensitive method that can analyze basal and near-basal expression of β-galactosidase in single *E. coli* BL21 (DE3) cells upon fluorescent staining with a fluorogenic substrate (89). **Figure 4** illustrates the detection principle and the gamma distribution fitted to the measured probability distribution of the β-galactosidase copy number without isopropyl β-D-thiogalactopyranoside (IPTG) induction, of which panel *a* represents the average frequency of expression bursts per cell cycle, and panel *b* denotes the average number of protein

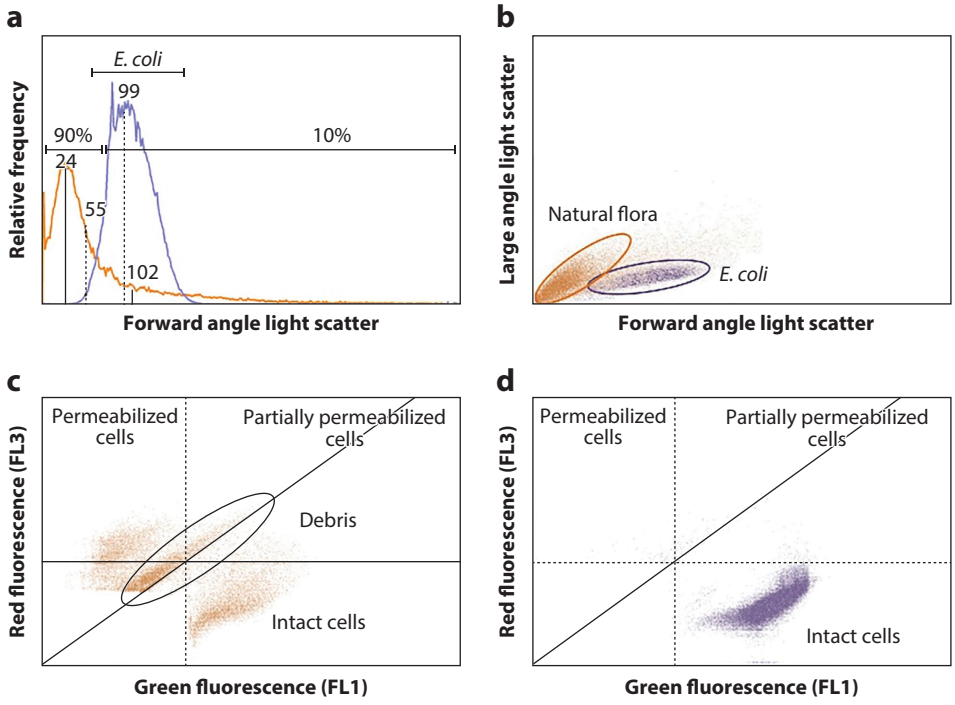

Figure 3

Flow cytometer profiling of untreated natural flora and *Escherichia coli* cells spiked on fresh-cut carrots after SYBR-I and PI staining. (*a*) Overlapping of forward angle light scatter histograms of natural flora and *E. coli* cells: the fraction percentage of small (90%) and large (10%) cells of natural flora are indicated. (*b*) Bivariate dot plot of forward angle light scatter versus large angle light scatter signals of natural flora and *E. coli* cells. (*c*) Bivariate dot plot of the green and red fluorescence (FL) signals of natural flora. (*d*) Bivariate dot plot of the green and red FL signals of *E. coli* cells. Figure adapted with permission from Reference 84. Copyright 2014, John Wiley & Sons.

molecules per burst (89). Employing β-lactamase-induced covalent labeling and immunofluorescent labeling, nFCM provides quantitative analysis of the resistant bacterial population down to 5% and 0.1%, respectively (90, 91). The measured dynamic population change confirmed that under the antimicrobial pressure, the original minority antibiotic-resistant bacteria outcompeted susceptible strains and became the dominant population after 5 h of growth. Meanwhile, detection of antibiotic-resistant infection in clinical urine samples was accomplished in less than 3 h without cultivation (91). Because production of β-lactamases that catalyze the hydrolysis of β-lactamase antibiotics is a major and threatening mechanism that confers antibiotic resistance, it is believed that nFCM-based quantitative methods hold great potential in the rapid diagnosis of antibiotic-resistant infection.

6. FLOW CYTOMETRIC ANALYSIS OF SINGLE MITOCHONDRIA

Mitochondria are double membrane–enclosed organelles responsible for the production of bioenergy and regulation of several cellular functions, such as apoptosis and autophagy (92, 93). Recent advances in mitochondria research have revealed the morphological and functional heterogeneity reflected by variations of mitochondrial metabolic state, lipid content, membrane potential,

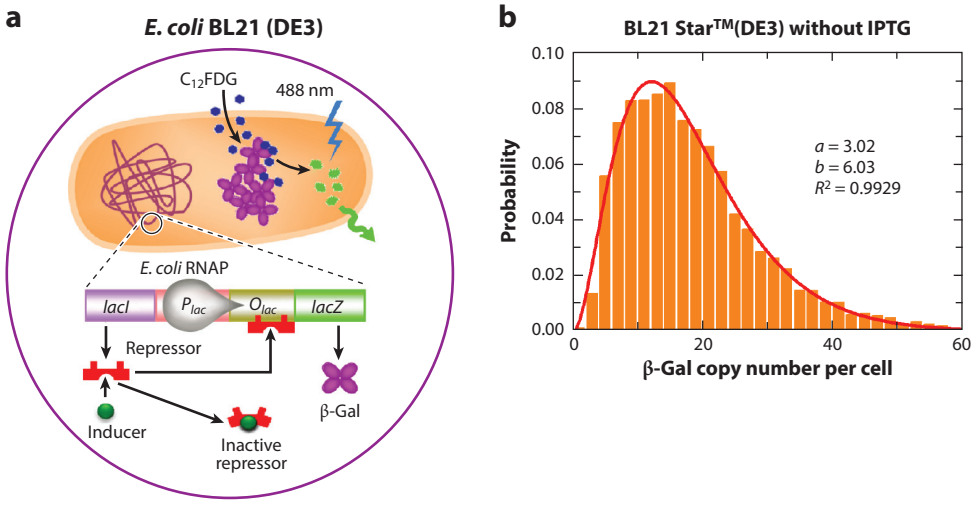

Figure 4

Flow cytometric analysis of basal level β-galactosidase (β-gal) expression in single bacterial cells. (*a*) Schematic diagram of β-gal expression at basal or near-basal levels under the control of a natural lac operon residing in the chromosome of *Escherichia coli* BL21 (DE3). (*b*) Gamma distribution fitted to the observed probability distribution of the β-gal copy number per cell in *E. coli* BL21 (DE3) without IPTG induction. Figure adapted with permission from Reference 89. Copyright 2013, Elsevier.

reactive oxygen species (ROS) production, mitochondrial DNA (mtDNA) copy number, calcium uptake, and protein expression level (94–97). Because such heterogeneity among individual mitochondria has been implicated in various physiological and pathological processes, including cell differentiation, aging, cancerization, and pharmaceutical resistance (98, 99), flow cytometric analysis of isolated mitochondria at the single-organelle level has become very attractive (100, 101). The advantage of multiparameter measurement of flow cytometry has been fully utilized to reveal the correlation among various biochemical and morphological properties and contents of an individual mitochondrion. For instance, simultaneous detection of membrane potential, volume, and cardiolipin content defined subpopulations of mitochondria with distinct morphological and functional properties in response to stressors (102). Besides, focusing on isolated mitochondria at the single-particle level eliminates the potential interference of other subcellular structures.

Although mitochondria are relatively large particles (0.5–1.0 μm in diameter), their small refractive indices impede the capability of a conventional flow cytometer from a complete discrimination of mitochondria against background by light-scattering detection. As demonstrated by our earlier research using the nFCM equipped with PMTs, the SSC intensity of a mitochondrion mainly fell between those of 100- to 200-nm polystyrene beads (**Figure 5*a***) (103). Meanwhile, the fluorescence-based measurement by conventional flow cytometry has been restricted to the mitochondrial attributes that can be brightly labeled, such as cardiolipin, ROS, membrane potential, and highly abundant mitochondrial proteins such as mitofusin2 (a surface protein involved in the mitochondrial fusion) (104–107). On the contrary, the poorly stained mitochondrial properties or contents, such as membrane potential of depolarized mitochondria or low-copy-number mitochondrial proteins (e.g., Bcl-2 family protein), thereby demand high-sensitivity instruments for discrimination.

Based on the unprecedented sensitivity of nFCM, we established a multiparameter correlation platform for a more definitive assessment of the purity, structural integrity, and apoptosis-related

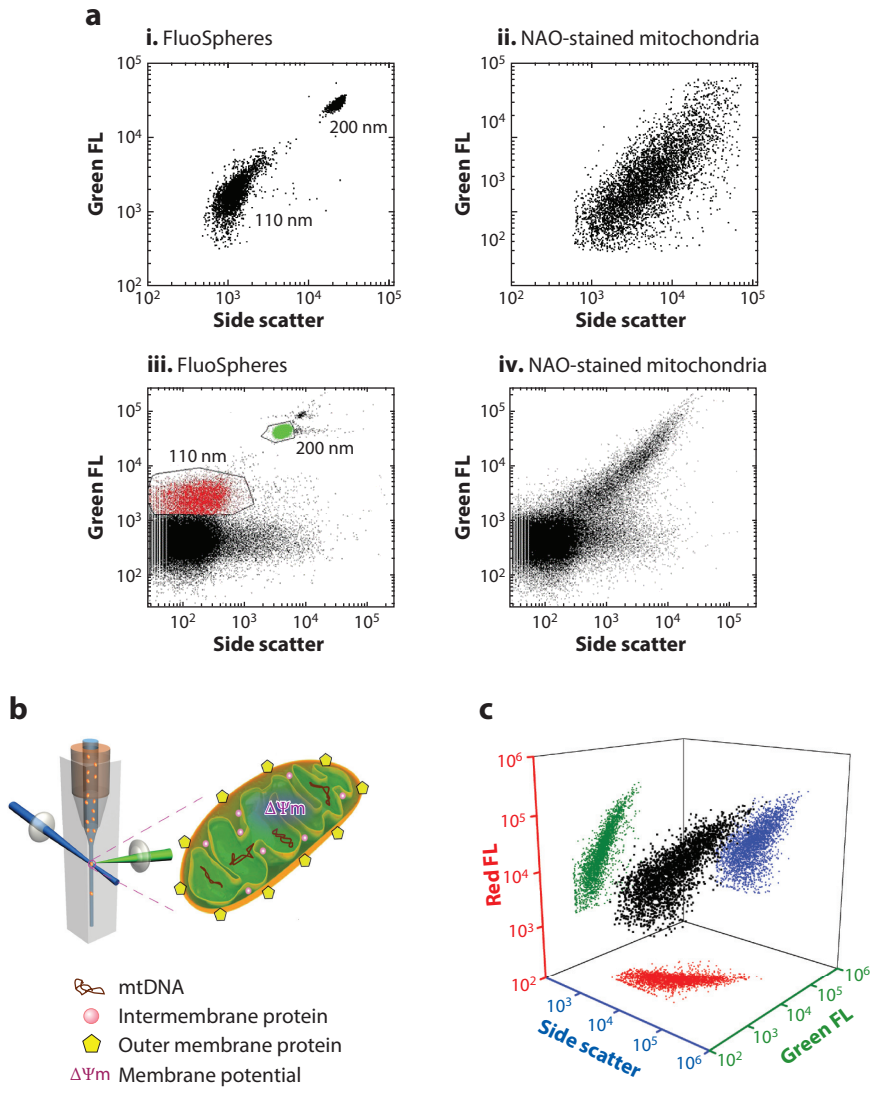

Figure 5

Flow cytometric analysis of single mitochondria. (*a*) Estimation of the sensitivity required for side scatter detection of single mitochondria by flow cytometry. (*b*) Schematic illustration of multiparameter analysis of single mitochondria by the nano-flow cytometer (nFCM). (*c*) Three-dimensional plot and the projected dot plots between side scatter and green fluorescence (FL) with different colors. Figure adapted with permission from Reference 103. Copyright 2012, American Chemical Society.

proteins of isolated mitochondria (**Figure 5*b,c***) (103). The SSC signal represented all of the detected particles, including intact and fragmented mitochondria, as well as other organelle debris produced during isolation procedures, while fluorescent signals from mtDNA, cardiolipin, cytochrome c, and porin indicated the existence of mitochondrial matrix, inner membrane, intermembrane space, and outer membrane, respectively. Taking advantage of this platform, we further developed an effective approach for quick identification of mitochondria-targeting anticancer compounds to induce apoptosis (108). This was achieved by detecting the membrane

potential collapse upon direct drug treatment on isolated mitochondria, indicated via fluorescent staining with $DiOC_6$ (3). Meanwhile, SSC detection reflected the structure change of single mitochondria upon drug stimulation. As a consequence, the different behaviors of eight drugs to alter mitochondrial morphology or membrane potential were verified to fit their different mechanisms for apoptosis induction. In our next study, the quantification of Bcl-2 family protein abundance and their variance under the normal state and upon apoptosis stimulation was reported for the first time (109). The results provided direct evidence of Bax translocation from cytosol to mitochondria, while no significant change of Bcl-2 content was observed upon apoptosis stimulation.

7. FLOW CYTOMETRIC ANALYSIS OF SINGLE VIRUSES

Despite the sensitivity limitation, flow cytometric analysis of viruses or virus-like particles, termed flow virometry, has become more mainstream recently (31, 110). In addition to the earlier application in environmental virus enumeration (111–113), flow virometry has already provided substantial information on the heterogeneity of viral particles in regard to their size (114, 115); integrity and aggregation (51, 115); genetic, lipid, and protein composition (114, 116–118); protein conformation (119); and even receptor-induced conformational changes (116). Such heterogeneity is highly relevant to virus sorting (114, 118), evaluation of viral fitness (e.g., maturation and infectivity) (116–120), and vaccine development and quality control (115, 121).

Due to the small particle sizes of viruses, fluorescence-based threshold triggering on a flow cytometer is often adopted through fluorescent labeling of genome with nucleic acid stains or proteins with antibodies, or envelope membrane with lipophilic dyes. Exemplary studies include the investigation of a variety of envelope protein conformations on individual HIV-1 virus (119), identification and quantification of infectious Junin virus harboring both envelope glycoprotein and RNA contents (114), exploration of the correlation between viral infectivity and lipid membrane composition at the budding site (114), and revelation of maturation state of individual Dengue virus particles from different cellular sources (117). Besides, viable viruses permit genetic engineering-based labeling, whereby viral components of interest are visualized by incorporation of fluorescence protein tags. For instance, recombinant HSV-1 viruses encoding green fluorescent protein (GFP)–tagged capsids, tegument proteins, and envelope proteins have been shown to be distinguishable over background by flow virometry, as reported by the Lippé group (118). The GFP tag incorporation is particularly useful for matrix/tegument protein inspection because these proteins are buried inside the envelope, rendering themselves not as amenable to the membrane permeabilization-free antibody labeling as glycoproteins on the envelope or capsid proteins of the nonenveloped viruses. However, such a large GFP moiety can be very perturbative to the recruitment of labeled proteins and the overall viral protein composition. Hence, novel genetic tagging tools have been added to the repertoire for labeling proteins of interest, such as small peptides or chemically modified amino acid, which allows for further visualization or detection upon fluorophore conjugation (122, 123).

Because most viruses are too small compared with the size of the focused laser spot, coincidence effects (swarm detection) are inclined to occur at high concentrations of samples, in which case multiple particles are interrogated simultaneously in the probe volume and counted as a single event. This results in underestimation of particle count, overestimation of particle brightness, and artifactual colocalization of fluorescent labels. For real single-virus analysis, a proper range of dilutions is required to ensure linear correlation between the dilution factor and the event count rate, whereas mean optical intensities remain unchanged (51, 117, 118).

Despite the fact that size heterogeneity of viruses can be revealed by flow virometry (114, 115), virus sizing had been quite challenging until the development of nFCM, which can detect single

a

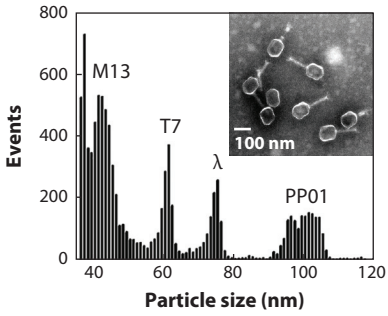

b

Viruses	EPD (nm)	nFCM (nm)	DLS (nm)
M13	38.9	41.8 ± 3.2	49.0 ± 16.9
T7	60.2	60.6 ± 1.3	57.4 ± 13.3
λ	64.2	74.4 ± 1.4	65.1 ± 15.0
PP01	96.5	99.6 ± 4.5	110.5 ± 29.0

Figure 6

Label-free analysis of single viruses. (*a*) Particle size distribution histogram with a bin width of 0.5 nm for the mixture of four different types of bacteriophages obtained by nFCM. (*Inset*) Electron microscopic analysis of bacteriophage PP01. (*b*) Comparison of the accuracy and precision of the TEM, nFCM, and DLS techniques in virus size measurements. Abbreviations: DLS, dynamic light scattering; EPD, equivalent particle diameter calculated from TEM analysis results; nFCM, nano-flow cytometer; TEM, transmission electron microscopy. Figure adapted with permission from Reference 10. Copyright 2016, John Wiley & Sons.

viruses as small as 27 nm (10). Through label-free analysis of single viruses, we reported virus sizing with a resolution comparable to that of electron microscopy. By focusing a 200-mW laser beam on a 6.4-μm spot, detection of MS2 viruses was achieved with an S/N of 11. Using monodisperse silica nanoparticles as a calibrator, the virus sizes obtained from the nFCM for bacteriophages M13, T7, λ, and PP01 agreed well with their structural dimensions reported in the literature via TEM or cryo-TEM characterization (**Figure 6**). Moreover, subtle structural difference of the same viral particles such as PP01 with retracted or extended tail fibers is resolvable. We expect to see a wider utility of nFCM in the detection and characterization of single viruses when versatile fluorescent labeling tools are used with it.

8. FLOW CYTOMETRIC ANALYSIS OF SINGLE EXTRACELLULAR VESICLES

EVs are nanoscale membrane vesicles secreted by cells to mediate intercellular communication via transfer of proteins, lipids, and nucleic acids (32). EVs are increasingly recognized as novel biomarkers for disease diagnosis and as efficient carriers for drug delivery. Depending on different biogenesis pathways, EVs are mainly classified as exosomes (30–100 nm) and microvesicles (or microparticles) (100–1,000 nm), respectively. Measurements by TEM (11, 124) and AFM (8) show that most EVs are smaller than 500 nm, which severely hampers the detection by light scattering–based flow cytometry.

In order to discriminate EVs from background, fluorescence labeling with lipid membrane dyes like PKH 67, annexin V (a molecule with affinity to phosphatidylserine-exposing EVs), or antibodies to specific surface antigens needs to be implemented. Based on fluorescence threshold triggering, an approximate EV detection limit of 100 nm was achieved by the Brisson group using a Beckman Coulter Gallios (125) and by the Wauben group using a modified BD influx (43, 44); an EV detection limit of 70–80 nm was realized by the Nolan group using a high-sensitivity flow cytometer custom constructed upon a BD FACSCanto (126). As reported by the Brisson group (125), fluorescence triggering enabled the detection of higher concentrations of EVs in

plasma than forward scattering–based triggering (40-fold for annexin V binding EVs, 75-fold for $CD41^+$ EVs, and 15-fold for $CD235a^+$ EVs). The Wauben group (43, 44) used PKH 67 to label EVs and emphasized the indispensable separation of unbound dye and dye aggregates from EVs, which will otherwise trigger events and elicit undesired variations into the measurement. Because dye washing requires time- and sample-consuming gradient ultracentrifugation, Stoner et al. (126) bypassed this wash step by optimizing dye and staining conditions. They selected di-8-ANEPPS, which outperformed other fluorescent lipid probes in fluorescence enhancement upon interaction with lipid membrane and intercalated into membrane vesicles in a stoichiometric manner.

Considering that the fluorescence intensity of di-8-ANEPPS is proportional to the surface area of labeled EVs, particle size distribution of EVs can be estimated. Although fluorescence-based triggering is helpful in distinguishing small EVs from the background, no generic marker can stain all EVs and only EVs. For example, observation on cryo-TEM revealed that approximately 50% of the total EVs from platelet-free plasma were annexin V negative (124). Recently, de Rond et al. (127) compared five commonly used fluorescent dyes for EV labeling: calcein AM, calcein violet, CFSE, di-8-ANEPPS, and lactadherin. None of the tested dyes fulfilled 100% sensitivity and specificity to EVs, and there was a large discrepancy in the performance of all the tested dyes when applied to EVs isolated from different origins. It is worth noting that because EVs are much smaller than the laser probe volume, attention must be paid to avoid the swarming detection by flow cytometry (25).

Although a microvesicle scatters 15 times less light than a 200-nm polystyrene bead of the same size owing to refractive index difference (41), light scattering–based detection of EVs remains attractive, as every EV particle scatters light. Once the scattered light can be discerned against background, it can be used as a hallmark of a particular event (that covers all EVs), and an EV staining ratio of a specific fluorescent labeling event can be evaluated. Using the scatter-diameter relationship based on the Mie model, van der Pol et al. (128) investigated the size range of detectable EVs among a wide variety of flow cytometers. They found that only a few highly sensitive instruments (including Apogee A50-Micro, BD influx, and BD LSR II) enabled the detection of 300- to 600-nm EVs, while the remaining conventional types, if applicable, are suitable for large EVs with ranges of 600–1,200 nm and/or 1,200–3,000 nm (**Figure 7**). By using the laboratory-built nFCM with extreme SSC sensitivity, we reported light-scattering detection of single EVs down to 40 nm (11). In this study, EVs isolated from colorectal cancer HCT15 cells were detected and accurately sized by using monodisperse silica nanoparticles as reference standards and upon refractive index mismatch correction. The particle size distribution profile obtained by nFCM was comparable in both accuracy and resolution to parallel cryo-TEM measurement (**Figure 8**). It was found that for EVs isolated from colorectal cancer HCT15 cells, most (97%) EVs are smaller than 150 nm. Subpopulations of EVs expressing CD9, CD63, and/or CD81 were quantified upon immunofluorescent staining. When EVs isolated from platelet-free plasma were analyzed, a significantly elevated level of CD147-positive EVs was identified in colorectal cancer patients compared to healthy controls. Therefore, nFCM offers an advanced platform for the quantitative and multiparameter analysis of individual EVs.

The refractive index of EVs is generally considered uniform and estimated as 1.400 when applied to the commonly used Mie model for EV sizing. However, it is more appropriate to describe EV as an intravesicular fluid with a low refractive index (1.38) that is surrounded by a phospholipid membrane with a high refractive index (1.48). In search of more suitable reference materials for EVs, researchers have proposed liposome and virus as candidates (129). Alternatively, Varga et al. (130) developed a hollow organosilica bead with a low-refractive-index core and high-refractive-index shell, which may scatter light comparably to EVs of similar diameter.

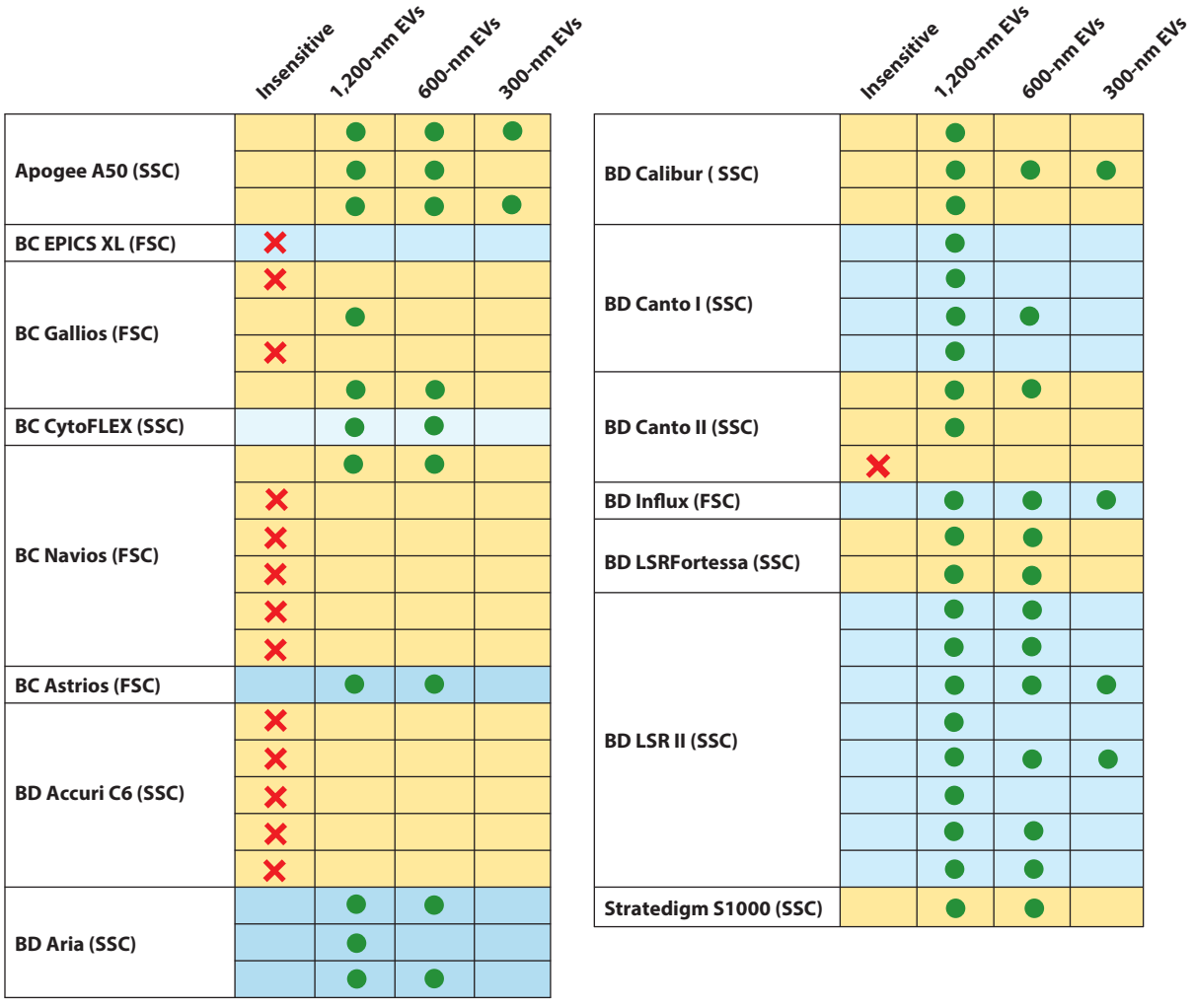

Figure 7

Assessment of flow cytometer (FCM) sensitivity. Green markers indicate whether an FCM was capable of detecting the signal of 1,200-nm, 600-nm, and/or 300-nm vesicles above the threshold level. Whether the model was applied to forward scatter (FSC) or side scatter (SSC) is shown in parentheses after the FCM name. Figure adapted with permission from Reference 128 under the terms of the Creative Commons Attribution Non-Commercial (CC BY-NC) License, **http://creativecommons.org/licenses/by/4.0**.

9. FUTURE PROSPECTS

Recent advances in high-sensitivity flow cytometry present new opportunities to measure the count, size, composition, phenotype, and physical state of nanoscale BPOs with unprecedented sensitivity and accuracy. These advantages enable investigators to reveal the identity and functions of BPOs, and more applications are expected. For example, little is known about ultramicrobacteria, the smallest bacteria, which are mainly observed by electron microscopy (131). High-sensitivity flow cytometry could provide a proficient tool to gain new insights into the physiology and function of ultramicrobacteria and their relationship with environment. The application of flow cytometry in EV analysis is just in its infancy. With the aid of ultrasensitive flow cytometry,

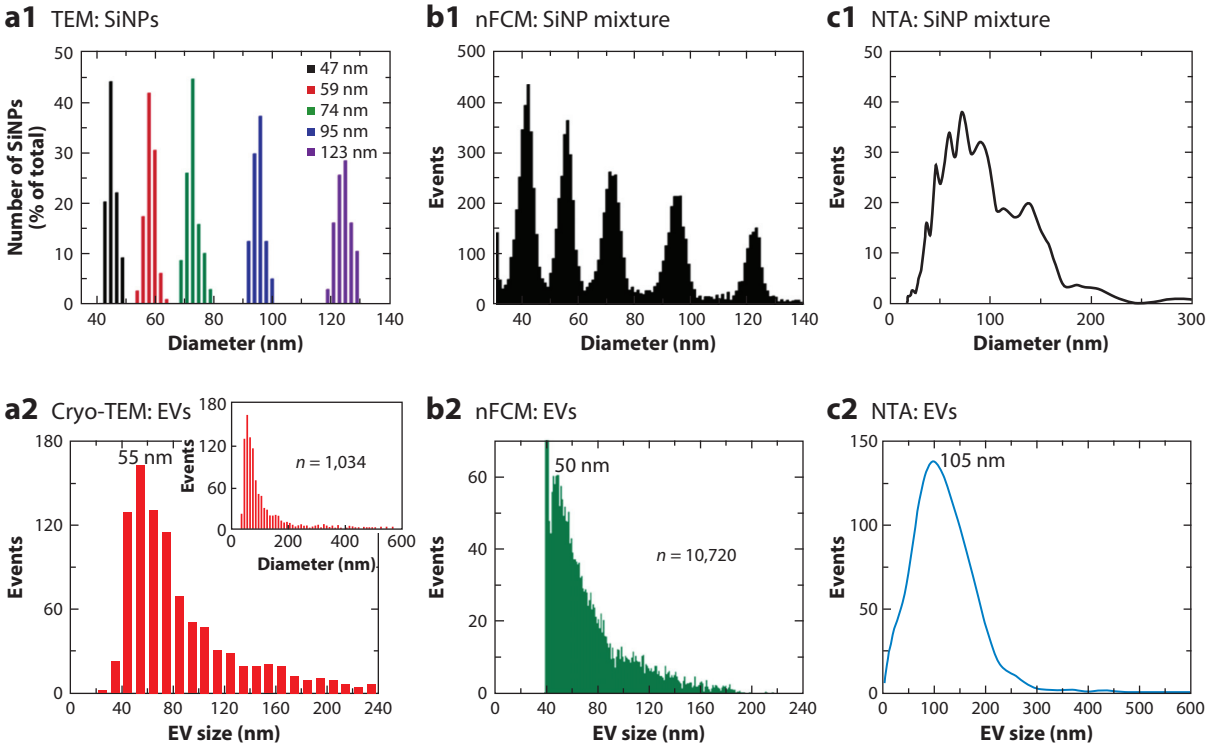

Figure 8

Resolution comparison among different techniques for nanoparticle sizing. (*a1*, *b1*, *c1*) Particle size distribution of SiNPs obtained by TEM, nFCM, and NTA. (*a2*, *b2*, *c2*) Particle size distribution of EVs obtained by cryo-TEM, nFCM, and NTA. Abbreviations: EV, extracellular vesicle; NTA, nanoparticle tracking analysis; SiNP, silicon nanoparticle; TEM, transmission electron microscopy. Figure adapted with permission from Reference 11. Copyright 2018, American Chemical Society.

more mechanistic roles of EVs in intercellular communication, tumor genesis, and disease diagnosis could be revealed. New analytical methods could be developed to discriminate viruses from EVs at the single-particle level, which can greatly assist the in-depth study of marine environments. Apart from the naturally occurring biological particles mentioned above, flow cytometric analysis of other subcellular structures such as chromosomes, ribosomes, and lysosomes, or of synthetic biofunctional nanoparticles, can be envisioned. Researchers in different fields could take advantage of ultrasensitive flow cytometers, such as the nFCM, to tackle biological problems that previously seemed intractable.

DISCLOSURE STATEMENT

X.Y. declares competing financial interests as a cofounder of NanoFCM Inc., a company committed to commercializing the nano-flow cytometry (nFCM) technology.

ACKNOWLEDGMENTS

This research was supported by the National Natural Science Foundation of China (grants 21627811, 21475112, and 21521004).

LITERATURE CITED

1. Brehm-Stecher BF, Johnson EA. 2004. Single-cell microbiology: tools, technologies, and applications. *Microbiol. Mol. Biol. Rev.* 68:538–59
2. Azam F, Malfatti F. 2007. Microbial structuring of marine ecosystems. *Nat. Rev. Microbiol.* 5:782–91
3. Norman TM, Lord ND, Paulsson J, Losick R. 2015. Stochastic switching of cell fate in microbes. *Annu. Rev. Microbiol.* 69:381–403
4. Koskella B, Hall LJ, Metcalf CJE. 2017. The microbiome beyond the horizon of ecological and evolutionary theory. *Nat. Ecol. Evol.* 1:1606–15
5. Levin-Reisman I, Ronin I, Gefen O, Braniss I, Shoresh N, Balaban NQ. 2017. Antibiotic tolerance facilitates the evolution of resistance. *Science* 355:826–30
6. Hagen C, Dent KC, Zeev-Ben-Mordehai T, Grange M, Bosse JB, et al. 2015. Structural basis of vesicle formation at the inner nuclear membrane. *Cell* 163:1692–701
7. Sun N, Malide D, Liu J, Rovira II, Combs CA, Finkel T. 2017. A fluorescence-based imaging method to measure *in vitro* and *in vivo* mitophagy using mt-Keima. *Nat. Protoc.* 12:1576–87
8. Yuana Y, Oosterkamp TH, Bahatyrova S, Ashcroft B, Garcia Rodriguez P, et al. 2010. Atomic force microscopy: a novel approach to the detection of nanosized blood microparticles. *J. Thromb. Haemost.* 8:315–23
9. Shpacovitch V, Temchura V, Matrosovich M, Hamacher J, Skolnik J, et al. 2015. Application of surface plasmon resonance imaging technique for the detection of single spherical biological submicrometer particles. *Anal. Biochem.* 486:62–69
10. Ma L, Zhu S, Tian Y, Zhang W, Wang S, et al. 2016. Label-free analysis of single viruses with a resolution comparable to that of electron microscopy and the throughput of flow cytometry. *Angew. Chem. Int. Ed.* 55:10239–43
11. Tian Y, Ma L, Gong M, Su G, Zhu S, et al. 2018. Protein profiling and sizing of extracellular vesicles from colorectal cancer patients via flow cytometry. *ACS Nano* 12:671–80
12. Yang L, Zhu S, Hang W, Wu L, Yan X. 2009. Development of an ultrasensitive dual-channel flow cytometer for the individual analysis of nanosized particles and biomolecules. *Anal. Chem.* 81:2555–63
13. Zhu S, Yang L, Long Y, Gao M, Huang T, et al. 2010. Size differentiation and absolute quantification of gold nanoparticles via single particle detection with a laboratory-built high-sensitivity flow cytometer. *J. Am. Chem. Soc.* 132:12176–78
14. Zhu S, Ma L, Wang S, Chen C, Zhang W, et al. 2014. Light-scattering detection below the level of single fluorescent molecules for high-resolution characterization of functional nanoparticles. *ACS Nano* 8:10998–1006
15. Spitzer MH, Nolan GP. 2016. Mass cytometry: single cells, many features. *Cell* 165:780–91
16. Chang Q, Ornatsky OI, Siddiqui I, Loboda A, Baranov VI, Hedley DW. 2017. Imaging mass cytometry. *Cytometry A* 91:160–69
17. Han Y, Gu Y, Zhang AC, Lo YH. 2011. Review: imaging technologies for flow cytometry. *Lab Chip* 16:4639–47
18. Doan M, Vorobjev I, Rees P, Filby A, Wolkenhauer O, et al. 2018. Diagnostic potential of imaging flow cytometry. *Trends Biotechnol.* 36:649–52
19. Yang RJ, Fu LM, Hou HH. 2018. Review and perspectives on microfluidic flow cytometers. *Sens. Actuators B* 266:26–45
20. Crosland-Taylor PJ. 1953. A device for counting small particles suspended in a fluid through a tube. *Nature* 171:37–38
21. Fulwyler MJ. 1965. Electronic separation of biological cells by volume. *Science* 150:910–11
22. Van Dilla MA, Trujillo TT, Mullaney PF, Coulter JR. 1969. Cell microfluorometry: a method for rapid fluorescence measurement. *Science* 163:1213–14
23. Shapiro HM. 2003. *Practical Flow Cytometry*. New York: Wiley-Liss
24. Steen HB. 2004. Flow cytometer for measurement of the light scattering of viral and other submicroscopic particles. *Cytometry A* 57:94–99

25. van der Pol E, van Gemert MJ, Sturk A, Nieuwland R, van Leeuwen TG. 2012. Single versus swarm detection of microparticles and exosomes by flow cytometry. *J. Thromb. Haemost.* 10:919–30
26. Foladori P, Quaranta A, Ziglio G. 2008. Use of silica microspheres having refractive index similar to bacteria for conversion of flow cytometric forward light scatter into biovolume. *Water Res.* 42:3757–66
27. van der Pol E, Coumans FA, Grootemaat AE, Gardiner C, Sargent IL, et al. 2014. Particle size distribution of exosomes and microvesicles determined by transmission electron microscopy, flow cytometry, nanoparticle tracking analysis, and resistive pulse sensing. *J. Thromb. Haemost.* 12:1182–92
28. Chandler WL, Yeung W, Tait JF. 2011. A new microparticle size calibration standard for use in measuring smaller microparticles using a new flow cytometer. *J. Thromb. Haemost.* 9:1216–24
29. Proctor CR, Besmer MD, Langenegger T, Beck K, Walser J-C, et al. 2018. Phylogenetic clustering of small low nucleic acid-content bacteria across diverse freshwater ecosystems. *ISME J.* 12:1344–59
30. Katz A, Alimova A, Xu M, Rudolph E, Shah MK, et al. 2003. Bacteria size determination by elastic light scattering. *IEEE J. Sel. Top. Quantum Electron.* 9:277–87
31. Lippé R. 2018. Flow virometry: a powerful tool to functionally characterize viruses. *J. Virol.* 92:e01765-17
32. El Andaloussi S, Mäger I, Breakefield XO, Wood MJA. 2013. Extracellular vesicles: biology and emerging therapeutic opportunities. *Nat. Rev. Drug Discov.* 12:347–57
33. Bohren CF, Huffman DR. 1983. *Absorption and Scattering of Light by Small Particles*. New York: Wiley-VCH
34. Nolan JP, Jones JC. 2017. Detection of platelet vesicles by flow cytometry. *Platelets* 28:256–62
35. Melamed MR. 2001. A brief history of flow cytometry and sorting. *Methods Cell Biol.* 63:3–17
36. Shapiro HM. 2004. The evolution of cytometers. *Cytometry A* 58:13–20
37. Hercher M, Mueller W, Shapiro HM. 1979. Detection and discrimination of individual viruses by flow cytometry. *J. Histochem. Cytochem.* 27:350–52
38. Steen HB, Lindmo T. 1979. Flow cytometry: a high-resolution instrument for everyone. *Science* 204:403–4
39. Steen HB. 1986. Simultaneous separate detection of low angle and large angle light scattering in an arc lamp-based flow cytometer. *Cytometry* 7:445–49
40. Steen HB. 1990. Light scattering measurement in an arc lamp-based flow cytometer. *Cytometry* 11:223–30
41. van der Pol E, Hoekstra AG, Sturk A, Otto C, van Leeuwen TG, Nieuwland R. 2010. Optical and non-optical methods for detection and characterization of microparticles and exosomes. *J. Thromb. Haemost.* 8:2596–607
42. Poncelet P, Robert S, Bouriche T, Bez J, Lacroix R, Dignat-George F. 2016. Standardized counting of circulating platelet microparticles using currently available flow cytometers and scatter-based triggering: Forward or side scatter? *Cytometry A* 89:148–58
43. Nolte-'t Hoen ENM, van der Vlist EJ, Aalberts M, Mertens HC, Bosch BJ, et al. 2012. Quantitative and qualitative flow cytometric analysis of nanosized cell-derived membrane vesicles. *Nanomedicine* 8:712–20
44. van der Vlist EJ, Nolte-'t Hoen ENM, Stoorvogel W, Arkesteijn GJ, Wauben MH. 2012. Fluorescent labeling of nano-sized vesicles released by cells and subsequent quantitative and qualitative analysis by high-resolution flow cytometry. *Nat. Protoc.* 7:1311–26
45. Maas SL, de Vrij J, van der Vlist EJ, Geragousian B, van Bloois L, et al. 2015. Possibilities and limitations of current technologies for quantification of biological extracellular vesicles and synthetic mimics. *J. Control. Release* 200:87–96
46. Robert S, Lacroix R, Poncelet P, Harhouri K, Bouriche T, et al. 2012. High-sensitivity flow cytometry provides access to standardized measurement of small-size microparticles—brief report. *Arterioscler. Thromb. Vasc. Biol.* 32:1054–58
47. Poncelet P, Robert S, Bailly N, Garnache-Ottou F, Bouriche T, et al. 2015. Tips and tricks for flow cytometry-based analysis and counting of microparticles. *Transfus. Apher. Sci.* 53:110–26

48. Morales-Kastresana A, Telford B, Musich TA, McKinnon K, Clayborne C, et al. 2017. Labeling extracellular vesicles for nanoscale flow cytometry. *Sci. Rep.* 7:1878
49. Kibria G, Ramos EK, Lee KE, Bedoyan S, Huang S, et al. 2016. A rapid, automated surface protein profiling of single circulating exosomes in human blood. *Sci. Rep.* 6:36502
50. Foladori P, Bruni L, Tamburini S, Ziglio G. 2010. Direct quantification of bacterial biomass in influent, effluent and activated sludge of wastewater treatment plants by using flow cytometry. *Water Res.* 44:3807–18
51. Bonar MM, Tilton JC. 2017. High sensitivity detection and sorting of infectious human immunodeficiency virus (HIV-1) particles by flow virometry. *Virology* 505:80–90
52. Steinkamp JA, Fulwyler MJ, Coulter JR, Hiebert RD, Horney JL, Mullancy PF. 1973. A new multiparameter separator for microscopic particles and biological cells. *Rev. Sci. Instrum.* 44:1301–10
53. Crissman HA, Tobey RA. 1974. Cell-cycle analysis in 20 minutes. *Science* 184:1297–98
54. Steinkamp JA, Wilson JS, Saunders GC, Stewart CC. 1982. Phagocytosis: flow cytometric quantitation with fluorescent microspheres. *Science* 215:64–66
55. Keller RA, Ambrose WP, Goodwin PM, Jett JH, Martin JC, Wu M. 1996. Single molecule fluorescence analysis in solution. *Appl. Spectrosc.* 50:A12–32
56. Ambrose WP, Goodwin PM, Jett JH, Van OA, Werner JH, Keller RA. 1999. Single molecule fluorescence spectroscopy at ambient temperature. *Chem. Rev.* 99:2929–56
57. Keller RA, Ambrose WP, Arias AA, Cai H, Emory SR, et al. 2002. Analytical applications of single-molecule detection. *Anal. Chem.* 74:316A–24A
58. Dovichi NJ, Martin JC, Jett JH, Keller RA. 1983. Attogram detection limit for aqueous dye samples by laser-induced fluorescence. *Science* 219:845–47
59. Shera EB, Seitzinger NK, Davis LM, Keller RA, Soper SA. 1990. Detection of single fluorescent molecules. *Chem. Phys. Lett.* 174:553–57
60. Nguyen DC, Keller RA, Jett JH, Martin JC. 1987. Detection of single molecules of phycoerythrin in hydrodynamically focused flows by laser-induced fluorescence. *Anal. Chem.* 59:2158–61
61. Dovichi NJ, Martin JC, Jett JH, Trkula M, Keller RA. 1984. Laser-induced fluorescence of flowing samples as an approach to single-molecule detection in liquids. *Anal. Chem.* 56:348–54
62. Zhu S, Wang S, Yang L, Huang T, Yan X. 2011. Progress in the development of techniques based on light scattering for single nanoparticle detection. *Sci. China Chem.* 54:1244–53
63. Eckburg PB, Bik EM, Bernstein CN, Purdom E, Dethlefsen L, et al. 2005. Diversity of the human intestinal microbial flora. *Science* 308:1635–38
64. Martinez JL, Baquero F, Andersson DI. 2007. Predicting antibiotic resistance. *Nat. Rev. Microbiol.* 5:958–65
65. Lu H, Chandran K, Stensel D. 2014. Microbial ecology of denitrification in biological wastewater treatment. *Water Res.* 64:237–54
66. Tamburini S, Shen N, Wu HC, Clemente JC. 2016. The microbiome in early life: implications for health outcomes. *Nat. Med.* 22:713–22
67. Gagneux S. 2018. Ecology and evolution of *Mycobacterium tuberculosis*. *Nat. Rev. Microbiol.* 16:202–13
68. Ambriz-Aviña V, Contreras-Garduño JA, Pedraza-Reyes M. 2014. Applications of flow cytometry to characterize bacterial physiological responses. *Biomed. Res. Int.* 2014:461941
69. Léonard L, Bouarab Chibane L, Ouled Bouhedda B, Degraeve P, Oulahal N. 2016. Recent advances on multi-parameter flow cytometry to characterize antimicrobial treatments. *Front Microbiol.* 7:1225
70. Wu L, Wang S, Song Y, Wang X, Yan X. 2016. Applications and challenges for single-bacteria analysis by flow cytometry. *Sci. China Chem.* 59:30–39
71. Kennedy D, Wilkinson MG. 2017. Application of flow cytometry to the detection of pathogenic bacteria. *Curr. Issues Mol. Biol.* 23:21–38
72. Van NS, Koetzsch S, Proctor CR, Besmer MD, Prest EI, et al. 2017. Flow cytometric bacterial cell counts challenge conventional heterotrophic plate counts for routine microbiological drinking water monitoring. *Water Res.* 113:191–206
73. Bergquist PL, Hardiman EM, Ferrari BC, Winsley T. 2009. Applications of flow cytometry in environmental microbiology and biotechnology. *Extremophiles* 13:389–401

74. Wilkinson MG. 2015. *Flow Cytometry in Microbiology: Technology and Applications*. Poole, UK: Caister Acad.
75. Lee H, Hwang JS, Lee J, Kim JI, Lee DG. 2015. Scolopendin 2, a cationic antimicrobial peptide from centipede, and its membrane-active mechanism. *Biochim. Biophys. Acta* 1848:634–42
76. Morishige Y, Fujimori K, Amano F. 2015. Use of flow cytometry for quantitative analysis of metabolism of viable but non-culturable (VBNC) *Salmonella*. *Biol. Pharm. Bull.* 38:1255–64
77. Kramer B, Thielmann J. 2016. Monitoring the live to dead transition of bacteria during thermal stress by a multi-method approach. *J. Microbiol. Methods* 123:24–30
78. Massicotte R, Mafu AA, Ahmad D, Deshaies F, Pichette G, Belhumeur P. 2017. Comparison between flow cytometry and traditional culture methods for efficacy assessment of six disinfectant agents against nosocomial bacterial species. *Front. Microbiol.* 8:112
79. Klümper U, Riber L, Dechesne A, Sannazzarro A, Hansen LH, et al. 2015. Broad host range plasmids can invade an unexpectedly diverse fraction of a soil bacterial community. *ISME J.* 9:934–45
80. Tejerizo GT, Bañuelos LA, Cervantes L, Gaytán P, Pistorio M, et al. 2015. Development of molecular tools to monitor conjugative transfer in rhizobia. *J. Microbiol. Methods* 117:155–63
81. Wu L, Wang X, Zhang J, Luan T, Bouveret E, Yan X. 2017. Flow cytometric single-cell analysis for quantitative in vivo detection of protein–protein interactions via relative reporter protein expression measurement. *Anal. Chem.* 89:2782–89
82. Gasol JM, Giorgio PAD. 2000. Using flow cytometry for counting natural planktonic bacteria and understanding the structure of planktonic bacterial communities. *Sci. Mar.* 64:197–224
83. Vives-Rego J, Lebaron P, Nebe-von Caron G. 2000. Current and future applications of flow cytometry in aquatic microbiology. *FEMS Microbiol. Rev.* 24:429–48
84. Tamburini S, Foladori P, Ferrentino G, Spilimbergo S, Jousson O. 2014. Accurate flow cytometric monitoring of *Escherichia coli* subpopulations on solid food treated with high pressure carbon dioxide. *J. Appl. Microbiol.* 117:440–50
85. Yu M, Wu L, Huang T, Wang S, Yan X. 2015. Rapid detection and enumeration of total bacteria in drinking water and tea beverages using a laboratory-built high-sensitivity flow cytometer. *Anal. Methods* 7:3072–79
86. He S, Hong X, Huang T, Zhang W, Zhou Y, et al. 2017. Rapid quantification of live/dead lactic acid bacteria in probiotic products using high-sensitivity flow cytometry. *Methods Appl. Fluoresc.* 5:024002
87. Yang L, Wu L, Zhu S, Long Y, Hang W, Yan X. 2010. Rapid, absolute, and simultaneous quantification of specific pathogenic strain and total bacterial cells using an ultrasensitive dual-color flow cytometer. *Anal. Chem.* 82:1109–16
88. Yang L, Zhou Y, Zhu S, Huang T, Wu L, Yan X. 2012. Detection and quantification of bacterial autofluorescence at the single-cell level by a laboratory-built high-sensitivity flow cytometer. *Anal. Chem.* 84:1526–32
89. Yang L, Huang T, Zhu S, Zhou Y, Jiang Y, et al. 2013. High-throughput single-cell analysis of low copy number β-galactosidase by a laboratory-built high-sensitivity flow cytometer. *Biosens. Bioelectron.* 48:49–55
90. Shao Q, Zheng Y, Dong X, Tang K, Yan X, Xing B. 2013. A covalent reporter of β-lactamase activity for fluorescent imaging and rapid screening of antibiotic-resistant bacteria. *Chem. Eur. J.* 19:10903–10
91. Huang T, Zheng Y, Yan Y, Yang L, Yao Y, et al. 2016. Probing minority population of antibiotic-resistant bacteria. *Biosens. Bioelectron.* 80:323–30
92. Wagner BK, Kitami T, Gilbert TJ, Peck D, Ramanathan A, et al. 2008. Large-scale chemical dissection of mitochondrial function. *Nat. Biotechnol.* 26:343–51
93. Friedman JR, Nunnari J. 2014. Mitochondrial form and function. *Nature* 505:335–43
94. Kuznetsov AV, Margreiter R. 2009. Heterogeneity of mitochondria and mitochondrial function within cells as another level of mitochondrial complexity. *Int. J. Mol. Sci.* 10:1911–29
95. Keil VC, Funke F, Zeug A, Schild D, Müller M. 2011. Ratiometric high-resolution imaging of JC-1 fluorescence reveals the subcellular heterogeneity of astrocytic mitochondria. *Pflügers Arch.* 462:693–708

96. Ye X, Wang G, Huang G, Bian X, Qian G, Yu S. 2011. Heterogeneity of mitochondrial membrane potential: A novel tool to isolate and identify cancer stem cells from a tumor mass? *Stem Cell Rev*. 7:153–60
97. Chatre L, Ricchetti M. 2013. Large heterogeneity of mitochondrial DNA transcription and initiation of replication exposed by single-cell imaging. *J. Cell Sci.* 126:914–26
98. Nunnari J, Suomalainen A. 2012. Mitochondria: in sickness and in health. *Cell* 148:1145–59
99. Aryaman J, Hoitzing H, Burgstaller JP, Johnston IG, Jones NS. 2017. Mitochondrial heterogeneity, metabolic scaling and cell death. *Bioessays* 39:170001
100. Mattiasson G. 2004. Flow cytometric analysis of isolated liver mitochondria to detect changes relevant to cell death. *Cytometry A* 60:145–54
101. Cottet-Rousselle C, Ronot X, Leverve X, Mayol JF. 2011. Cytometric assessment of mitochondria using fluorescent probes. *Cytometry A* 79:405–25
102. Saunders JE, Beeson CC, Schnellmann RG. 2013. Characterization of functionally distinct mitochondrial subpopulations. *J. Bioenerg. Biomembr.* 45:87–99
103. Zhang S, Zhu S, Yang L, Zheng Y, Gao M, et al. 2012. High-throughput multiparameter analysis of individual mitochondria. *Anal. Chem.* 84:6421–28
104. Petit PX, O'Connor JE, Grunwald D, Brown SC. 1990. Analysis of the membrane-potential of rat-liver and mouse-liver mitochondria by flow-cytometry and possible applications. *Eur. J. Biochem.* 194:389–97
105. Medina JM, López-Mediavilla C, Orfao A. 2002. Flow cytometry of isolated mitochondria during development and under some pathological conditions. *FEBS Lett*. 510:127–32
106. Lee DR, Helps SC, Macardle PJ, Nilsson M, Sims NR. 2009. Alterations in membrane potential in mitochondria isolated from brain subregions during focal cerebral ischemia and early reperfusion: evaluation using flow cytometry. *Neurochem. Res.* 34:1857–66
107. Pickles S, Arbour N, Vande Velde C. 2014. Immunodetection of outer membrane proteins by flow cytometry of isolated mitochondria. *J. Vis. Exp.* 91:51887
108. Zhang X, Zhang S, Zhu S, Chen S, Han J, et al. 2014. Identification of mitochondria-targeting anticancer compounds by an in vitro strategy. *Anal. Chem.* 86:5232–37
109. Chen C, Zhang X, Zhang S, Zhu S, Xu J, et al. 2015. Quantification of protein copy number in single mitochondria: the Bcl-2 family proteins. *Biosens. Bioelectron.* 74:476–82
110. Zamora JLR, Aguilar HC. 2018. Flow virometry as a tool to study viruses. *Methods* 134–135:87–97
111. Marie D, Brussaard CPD, Thyrhaug R, Bratbak G, Vaulot D. 1999. Enumeration of marine viruses in culture and natural samples by flow cytometry. *Appl. Environ. Microbiol.* 65:45–52
112. Brussaard CP. 2004. Optimization of procedures for counting viruses by flow cytometry. *Appl. Environ. Microbiol.* 70:1506–13
113. Brown MR, Camezuli S, Davenport RJ, Petelenz-Kurdziel E, Ovreas L, Curtis TP. 2015. Flow cytometric quantification of viruses in activated sludge. *Water Res.* 68:414–22
114. Gaudin R, Barteneva NS. 2015. Sorting of small infectious virus particles by flow virometry reveals distinct infectivity profiles. *Nat. Commun.* 6:6022
115. Tang VA, Renner TM, Varette O, Le Boeuf F, Wang J, et al. 2016. Single-particle characterization of oncolytic vaccinia virus by flow virometry. *Vaccine* 34:5082–89
116. Landowski M, Dabundo J, Liu Q, Nicola AV, Aguilar HC. 2014. Nipah virion entry kinetics, composition, and conformational changes determined by enzymatic virus-like particles and new flow virometry tools. *J. Virol.* 88:14197–206
117. Zicari S, Arakelyan A, Fitzgerald W, Zaitseva E, Chernomordik LV, et al. 2016. Evaluation of the maturation of individual Dengue virions with flow virometry. *Virology* 488:20–27
118. El Bilali N, Duron J, Gingras D, Lippé R. 2017. Quantitative evaluation of protein heterogeneity within herpes simplex virus 1 particles. *J. Virol.* 91:e00320-17
119. Arakelyan A, Fitzgerald W, King DF, Rogers P, Cheeseman HM, et al. 2017. Flow virometry analysis of envelope glycoprotein conformations on individual HIV virions. *Sci. Rep.* 7:948
120. Wargo AR, Kurath G. 2012. Viral fitness: definitions, measurement, and current insights. *Curr. Opin. Virol.* 2:538–45

121. Vlasak J, Hoang VM, Christanti S, Peluso R, Li F, Culp TD. 2016. Use of flow cytometry for characterization of human cytomegalovirus vaccine particles. *Vaccine* 34:2321–28
122. Wu L, Huang T, Yang L, Pan J, Zhu S, Yan X. 2011. Sensitive and selective bacterial detection using tetracysteine-tagged phages in conjunction with biarsenical dye. *Angew. Chem. Int. Ed.* 50:5873–77
123. Zhang C, Zhou X, Yao T, Tian Z, Zhou D. 2018. Precision fluorescent labeling of an adeno-associated virus vector to monitor the viral infection pathway. *Biotechnol. J.* 13:e1700374
124. Arraud N, Linares R, Tan S, Gounou C, Pasquet JM, et al. 2014. Extracellular vesicles from blood plasma: determination of their morphology, size, phenotype and concentration. *J. Thromb. Haemost.* 12:614–27
125. Arraud N, Gounou C, Turpin D, Brisson AR. 2016. Fluorescence triggering: a general strategy for enumerating and phenotyping extracellular vesicles by flow cytometry. *Cytometry A* 89:184–95
126. Stoner SA, Duggan E, Condello D, Guerrero A, Turk JR, et al. 2016. High sensitivity flow cytometry of membrane vesicles. *Cytometry A* 89:196–206
127. de Rond L, van der Pol E, Hau CM, Varga Z, Sturk A, et al. 2018. Comparison of generic fluorescent markers for detection of extracellular vesicles by flow cytometry. *Clin. Chem.* 64:680–89
128. van der Pol E, Sturk A, van Leeuwen T, Nieuwland R, Coumans F. 2018. Standardization of extracellular vesicle measurements by flow cytometry through vesicle diameter approximation. *J. Thromb. Haemost.* 16:1236–45
129. Valkonen S, van der Pol E, Boing A, Yuana Y, Yliperttula M, et al. 2017. Biological reference materials for extracellular vesicle studies. *Eur. J. Pharm. Sci.* 98:4–16
130. Varga Z, van der Pol E, Pálmai M, Garcia-Diez R, Gollwitzer C, et al. 2018. Hollow organosilica beads as reference particles for optical detection of extracellular vesicles. *J. Thromb. Haemost.* 16:1646–55
131. Duda VI, Suzina NE, Polivtseva VN, Boronin AM. 2012. Ultramicrobacteria: formation of the concept and contribution of ultramicrobacteria to biology. *Microbiology* 81:379–90